Original Article

Novel Insights into the Aortic Mechanical Properties of Mice Modeling Hereditary Aortic Diseases

Nicolo Dubacher, Kaori Sugiyama, Jeffrey D. Smith, Vanessa Nussbaumer, Máté Csonka, Szilamér Ferenczi, Krisztina J. Kovács, Sylvan M. Caspar, Lisa Lamberti, Janine Meienberg, Hiromi Yanagisawa*, Mary B. Sheppard*, Gabor Matyas*

Affiliations

Center for Cardiovascular Genetics and Gene Diagnostics, Swiss Foundation for People with Rare Diseases, Switzerland (N.D., V.N., M.C., S.M.C., L.L., J.M., G.M.), Translational Cardiovascular Technologies, Department of Health Sciences, ETH Zurich, Switzerland (N.D.), Institute for Advanced Research of Biosystem Dynamics, Research Institute for Science and Engineering, Waseda University, Japan (K.S.), Life Science Center for Survival Dynamics, Tsukuba Advanced Research Alliance, University of Tsukuba, Japan (K.S., H.Y.), Saha Cardiovascular Research Center, University of Kentucky, USA (J.D.S.), Heart and Vascular Center, Semmelweis University, Hungary (M.C.), Laboratory of Molecular Neuroendocrinology, Institute of Experimental Medicine, Hungary (S.F., K.J.K.), Department of Family and Community Medicine, University of Kentucky, USA (M.B.S.), Saha Aortic Center, University of Kentucky, USA (M.B.S.), and Zurich Center for Integrative Human Physiology, University of Zurich, Switzerland (G.M.).

*H. Yanagisawa, M.B. Sheppard, and G. Matyas are joint senior authors.

Short title: Aortic Rupture Force in Mice Modeling Aortic Diseases

Correspondence to: Gabor Matyas, PhD, Center for Cardiovascular Genetics and Gene Diagnostics, Swiss Foundation for People with Rare Diseases, Wagistrasse 25, 8952 Schlieren-Zurich, Switzerland. Email matyas@genetikzentrum.ch, Phone +41-43-433-86-86

ABSTRACT

OBJECTIVE: Hereditary aortic diseases (hADs) increase the risk of aortic dissections and ruptures. Recently, we have established an objective approach to measure the rupture force of the murine aorta, thereby explaining the outcomes of clinical studies and assessing the added value of approved drugs in vascular Ehlers-Danlos syndrome (vEDS). Here, we applied our approach to six additional mouse hAD models.

APPROACH AND RESULT: We used two mouse models of Marfan syndrome (MFS) as well as one smooth-muscle-cell-specific knockout (SMKO) of *Efemp2* and three CRISPR/Cas9-engineered knock-in models (*Ltbp1*, *Mfap4*, and *Timp1*). One of the two MFS models was subjected to 4-week-long losartan treatment. Per mouse, three rings of the thoracic aorta were prepared, mounted on a tissue puller, and uniaxially stretched until rupture. The aortic rupture force of the SMKO and both MFS models was significantly lower compared with wild-type mice but in both MFS models higher than in mice modeling vEDS. In contrast, the *Ltbp1*, *Mfap4*, and *Timp1* knock-in models presented no impaired aortic integrity. As expected, losartan treatment reduced aneurysm formation but surprisingly had no impact on the aortic rupture force of our MFS mice.

CONCLUSIONS: Our read-out system can characterize the aortic biomechanical integrity of mice modeling not only vEDS but also related hADs, allowing the aortic-rupture-force-focused comparison of mouse models. Furthermore, aneurysm progression alone may not be a sufficient read-out for aortic rupture, as antihypertensive drugs reducing aortic dilatation might not strengthen the weakened aortic wall. Our results may enable identification of improved medical therapies of hADs.

Key Words: aortic aneurysm, dissection, rupture, biomechanical integrity, *Efemp2*, *Fbn1*, Marfan syndrome

56 **Nonstandard Abbreviations and Acronyms**

hAD(s)	hereditary aortic disease(s)
AGTR1	angiotensin II receptor type 1
Col3a1	collagen, type III, alpha-1 (encoding gene in mice)
ECM	extracellular matrix
Efemp2	fibulin-4 (Fbln4) (encoding gene in mice)
Fbn1	fibrillin-1 (encoding gene in mice)
Ltbp1	latent TGF-β binding protein 1 (encoding gene in mice)
Mfap4	microfibril associated protein 4 (encoding gene in mice)
MFS	Marfan syndrome
MMP	matrix metalloproteinase
SMKO	smooth-muscle-specific knockout ($Efemp2^{loxP/KO}$;$SM22\text{-}Cre^{Tg/Tg}$)
TAA(s)	thoracic aortic aneurysm(s)
TGF	transforming growth factor
Timp1	tissue inhibitor of matrix metalloproteinase 1 (encoding gene in mice)
vEDS	vascular Ehlers-Danlos syndrome
WGS	whole-genome sequencing

57

58 Hereditary aortic diseases (hADs) with life-threatening aneurysms and dissections are
59 associated with high morbidity and mortality and are the cause for up to ~2% of all deaths in
60 the Western world.[1] Syndromic and non-syndromic forms of hADs are rare (i.e., prevalence
61 <1:2000) but several types have been identified so far. Despite considerable phenotypic
62 similarity, disease management can profoundly differ depending on the causative gene,
63 requiring molecular genetic testing.[2,3] The advent of high-throughput sequencing has enabled
64 genetic data generation at hitherto unprecedented scale, allowing for novel insights into the
65 molecular etiology of hereditary aortopathies but requiring a high level of expertise for
66 appropriate data analysis and variant interpretation.[4] Currently, at least 50 genes have been

67 associated with hereditary thoracic aortic aneurysms (TAAs) and classified based on the
68 strength of association.[5] However, these genes cannot explain all the cases of heritable TAAs,
69 suggesting the presence of additional causative genes for hADs.[6]

70 Changes in the structural components of the extracellular matrix (ECM) as well as in
71 chemical and mechanical stimuli can influence the molecular signaling pathways that regulate
72 aortic wall homeostasis. Accordingly, hAD-causing sequence variants (mutations) can affect
73 proper ECM organization, thereby directly impacting the mechanical properties of the aorta as
74 well as the mechanoregulation of vascular smooth muscle cells and their ability to sense
75 matrix-mediated mechanical stimuli.[7] This can result in impaired aortic integrity and
76 mechanical dysfunction causing progressive weakening of the aortic wall, ultimately leading
77 to arterial dissection and/or rupture.[8] The mechanical properties of the thoracic aorta can be
78 derived from *in vivo* imaging parameters such as aortic wall distensibility and local pulse
79 wave velocity or studied directly in *ex vivo* aortic samples.[9-11] In humans, however, studies
80 assessing the clinically relevant parameter of aortic rupture (with or without
81 aneurysm/dissection) in hAD are significantly limited. Thus, non-human models harboring
82 disease-causing variants in hAD-associated gene(s) provide a valuable alternative, when
83 combined with an appropriate read-out at individual level.

84 Recently, we have established an objective approach to measure the aortic rupture
85 force (maximum tensile force) of uniaxially stretched murine thoracic aortic rings as a read-
86 out for the biomechanical integrity of the aorta.[12] We have previously used this approach to
87 clarify whether or not antihypertensive drugs can also strengthen the thoracic aorta (i.e.,
88 increase rupture force), thereby showing that celiprolol, a 3rd-generation β-blocker, but not
89 losartan, an angiotensin-II-receptor-type-1 (AGTR1) inhibitor, can improve the
90 biomechanical integrity of the aortic wall (i.e., beyond the celiprolol's expected effect of
91 slowing heart rate and lowering blood pressure).[12] Accordingly, our approach provided a
92 possible explanation for the previous outcomes of clinical and retrospective studies in

93 vascular Ehlers-Danlos syndrome (vEDS, OMIM #130050).[13-15] This added value of
94 celiprolol, however, cannot simply be extrapolated to other β-blockers, as we have previously
95 demonstrated for bisoprolol.[16]

96 Here, we applied our established read-out approach[12] to measure the aortic rupture
97 force in six additional mouse hAD models and compared their aortic rupture force with that of
98 vEDS mice: (i) We used the two most widely investigated mouse models of Marfan syndrome
99 (MFS, OMIM #154700) (*Fbn1*^{C1041G} and *Fbn1*^{mgR}),[17-19] a rare autosomal-dominant inherited
100 disease with severe cardiovascular manifestations, such as TAAs predisposing to aortic
101 dissection and rupture, caused by mutations in the gene encoding fibrillin-1 (*FBN1* in
102 humans, *Fbn1* in mice).[20] In one of the two mouse MFS models (*Fbn1*^{mgR}), we also aimed to
103 clarify whether or not the frequently prescribed losartan, which has been shown to slow down
104 aneurysm progression in mouse models as well as humans with MFS,[21-25] also strengthens the
105 potentially weakened thoracic aorta. (ii) Furthermore, we assessed the aortic rupture force in
106 an *Efemp2* (encoding fibulin-4 [Fbln4]) smooth-muscle-specific knock-out (SMKO) model
107 recapitulating key vascular phenotypic features (aortic aneurysms and arterial tortuosity)[26] of
108 the autosomal-recessive inherited connective tissue disorder cutis laxa type 1B (OMIM
109 #614437).[27,28] (iii) Moreover, we used three novel CRISPR/Cas9-engineered knock-in models
110 (*Ltbp1*^{G1132S}, *Mfap4*^{D42A}, *Timp1*^{I120T}) to assess the causality of human-equivalent variants in
111 hAD candidate genes detected by whole-genome sequencing (WGS).[6]

112

METHODS

Mouse strains

In this study, multiple mouse strains were used. An overview can be found in the Major Resources Table in the Supplemental Material. Wild-type mice are referred to as $^{+/+}$.

Fbn1^{C1041G} and *Fbn1*^{mgR} Mouse Models

For the *Fbn1*^{C1041G} mouse model (C57BL/6J background), 10-week-old heterozygous (*Fbn1*$^{+/C1041G}$, n=10) and wild-type (*Fbn1*$^{+/+}$, n=10) mice were ordered in frozen condition from Jackson Laboratory (JAX stock #012885, Bar Harbor, ME, USA). Tail biopsies were taken to confirm the genotypes of delivered mice, for which DNA extraction, PCR, and subsequent Sanger sequencing were performed as previously described.[12,17]

Fbn1^{mgR} mice (C57BL/6J background) were bred and maintained on a 14/10-hour light/dark cycle receiving standard rodent chow and water *ad libitum*. Mice were genotyped as described previously.[18] In addition, 4-week-old homozygous (*Fbn1*$^{mgR/mgR}$, n=12) and wild-type (*Fbn1*$^{+/+}$, n=10) mice were treated for 4 weeks with losartan dissolved in drinking water at a concentration of 600 mg/L (LTK Labs, St. Paul, MN, USA, ~180 mg/kg bodyweight per day); age-matched, untreated *Fbn1*$^{mgR/mgR}$ (n=17) and *Fbn1*$^{+/+}$ (n=10) littermates receiving normal drinking water served as controls. Animals were weighed at the beginning and at the end of the treatment and water consumption was monitored regularly to ensure that control and treated mice drank comparable quantities. At the end of the treatment, mice were euthanized using CO_2 and subsequently frozen. Treatment protocols were approved by the University of Kentucky IACUC (approval reference number: 2016-2437) in line with the local guidelines.

137 ***Efemp2* SMKO Model**

138 *Efemp2*$^{loxP/KO}$;*SM22-Cre*$^{Tg/Tg}$ (SMKO) and wild-type littermates (wild-type for *Efemp2* but
139 containing the SM22α-Cre transgene, *Efemp2*$^{+/+}$;*SM22-Cre*$^{Tg/Tg}$) with a mixed genetic
140 background (C57BL/6J; 129SvEv) were bred and maintained on a 12-hour light/dark cycle
141 receiving standard rodent chow and water *ad libitum*. Genotyping was performed as
142 previously described.[26] Wild-type (n=11) and SMKO (n=11) littermates were euthanized with
143 CO_2 at 8 weeks of age and subsequently frozen. Animal experimentation and maintenance
144 were in accordance with and approved by the Institutional Animal Experiment Committee of
145 the University of Tsukuba, Japan (approval reference number: 21-108).

146

147 **CRISPR/Cas9-Engineered Mouse Models**

148 Three CRISPR/Cas9 knock-in mouse models (*Ltbp1*^{emG1132S}, *Mfap4*^{emD42A}, and *Timp1*^{emI120T})
149 were generated on the C57BL/6NJ background by Cyagen (Santa Clara, CA, USA), thereby
150 introducing human-equivalent sequence variants detected in our WGS cohort of hAD patients
151 (GRCm38/mm10 chr17(Ltbp1):g.75,315,062G>A, chr11(Mfap4):g.61,486,071A>C, and
152 chrX(Timp1):g.20,873,395T>C, modeling human variants *LTBP1* NM_206943.4: c.3418G>A
153 p.(Gly1140Ser), *MFAP4* NM_001198695.2: c.191A>C p.(Asp64Ala), and *TIMP1*
154 NM_003254.3: c.356T>C p.(Ile119Thr), respectively). Founder mice of the three strains were
155 bred and maintained on a 12-hour light/dark cycle receiving standard rodent chow and water
156 *ad libitum*. The genotype was determined after weaning at the age of 4 weeks by PCR and
157 subsequent Sanger sequencing using genomic DNA extracted of ear biopsies as previously
158 described.[12] Primers used for PCR and sequencing are listed in Table S1. One-year-old
159 heterozygous (*Ltbp1*$^{+/G1132S}$, n=10; *Mfap4*$^{+/D42A}$, n=10; *Timp1*$^{+/I120T}$, n=7), homozygous
160 (*Ltbp1*$^{G1132S/G1132S}$, n=10; *Mfap4*$^{D42A/D42A}$, n=8; *Timp1*$^{I120T/I120T}$, n=5), and hemizygous
161 (*Timp1*$^{0/I120T}$, n=9) mice as well as age-matched wild-type littermates serving as controls
162 (*Ltbp1*$^{+/+}$, n=10; *Mfap4*$^{+/+}$, n=9; *Timp1*$^{+/+}$, n=8) were euthanized with CO_2 and subsequently

frozen (cf. one-year-old mice were used to be able to detect any late-onset effects of the variants). Animal experimentation and maintenance were in accordance with institutional and local guidelines (approval reference number: ZH107/17, Zurich, Switzerland) conforming to the EU Directive 2010/63/EU for animal experiments.

Aortic Rupture Force Measurements

Euthanized mice kept in a frozen state were thawed immediately before measurement of aortic rupture force. For all mouse models, the maximum tensile force at rupture (in mN) of three uniaxially stretched 1.5-mm thoracic aortic rings/segments (segment S1, ascending aorta, after heart; segment S2, descending aorta, after aortic arch; segment S3, descending aorta, adjacent to S2; cf. graphical abstract and note that S1-S3 are ring-shaped) per mouse was measured and relative rupture force was calculated by setting the arithmetic mean of the respective wild-type S1 to 100% as previously described.[12] The stretching positions of the tissue puller until both 5 mN (load-free aortic diameter) and maximum force (rupture of aortic segment) were determined (in µm) as moved distance of the mounting pins during stretching. Mice were randomized and all measurements were performed blinded for the investigator.

Statistical Analyses

For arithmetic means, 95% confidence intervals (CIs) were calculated using two-tailed critical values of *t*-distribution (vassarstats.net/conf_mean.html). For means with non- or slightly (<2% of means) overlapping 95% CIs compared in the text, two-tailed *P* values were calculated by two-sample *t*-test (equal sample variances according to *F*-test) or Welch's *t*-test (unequal sample variances according to *F*-test), assuming normal distribution of independent samples (vassarstats.net/tu.html). For proportions, 95% CIs were calculated with continuity correction (vassarstats.net/prop1.html). For additional information, see Supplemental Material.

188 # RESULTS

189 ## *Fbn1*^{C1041G} Mouse Model

190 Compared to *Fbn1*$^{+/+}$ mice, the aortic rupture force of *Fbn1*$^{+/C1041G}$ mice was significantly
191 decreased in all three aortic segments (S1, S2, and S3) (Figure 1A; Table S2). No significant
192 difference in stretch was detected for any of the three aortic segments of 10-week-old *Fbn1*$^{+/+}$
193 and *Fbn1*$^{+/C1041G}$ mice when stretch was measured at 5 mN or maximum force (Figure 1B;
194 Tables S3 and S4). The relative aortic rupture force and stretch values of *Fbn1*$^{+/+}$ and
195 *Fbn1*$^{+/C1041G}$ mice were comparable in both sexes (Figure S1).

196

197 ## *Fbn1*^{mgR} Mouse Model

198 During 4 weeks of losartan treatment started at 4 weeks of age, the mortality rate of treated
199 *Fbn1*$^{mgR/mgR}$ mice (8.3% [95% CI, 0.4%-40.2%]) was not significantly lower than that of
200 untreated *Fbn1*$^{mgR/mgR}$ mice (11.8% [95% CI, 2.1%-37.7%]), but no wild-type littermate mice
201 died (Figure 2A). On average, males were heavier than females, but body weight did not
202 differ significantly between untreated and treated mice of the same sex and genotype either
203 before initiation of treatment (at 4 weeks of age) or after 4 weeks of treatment (at 8 weeks of
204 age) (Figure 2B). Of note, *Fbn1*$^{mgR/mgR}$ males were heavier than wild-type males (Figure 2B),
205 which is unexpected considering the human MFS phenotype but has been previously observed
206 in this mouse model and is attributed to altered adipose tissue homeostasis.[29]

207 Compared with untreated *Fbn1*$^{+/+}$ mice, the aortic rupture force was significantly
208 decreased in all three aortic segments of both untreated and losartan-treated *Fbn1*$^{mgR/mgR}$ mice,
209 also revealing that losartan did not strengthen the weakened aortic wall of *Fbn1*$^{mgR/mgR}$ mice
210 (Figure 3A; Table S5; Figure S2). The stretch of aortic segment S1 at both 5 mN and
211 maximum force was significantly increased in untreated *Fbn1*$^{mgR/mgR}$ mice compared to
212 untreated *Fbn1*$^{+/+}$ mice, which was more pronounced in males (Figure 3B; Tables S6 and S7).
213 While losartan treatment of *Fbn1*$^{+/+}$ mice had no effect on S1 stretch (Figure 3B; Tables S6

214 and S7), losartan treatment reduced S1 stretch at both 5 mN and maximum force in
215 *Fbn1*$^{mgR/mgR}$ mice regardless of sex (Figure 3B; Tables S6 and S7; in S2 and S3 there were no
216 considerable differences in stretch, so these data are not shown). Overall, our data
217 demonstrates that losartan did not significantly alter S1-S3 rupture force but did affect S1
218 stretch in *Fbn1*$^{mgR/mgR}$ mice modeling MFS.
219
220 ***Efemp2* SMKO Mouse Model**
221 Compared to wild-type mice, our measurements showed significantly reduced relative aortic
222 rupture force in the ascending thoracic aorta (S1) but no difference in the descending aorta
223 (S2 and S3) of SMKO mice (Figure 4A; Table S8). Furthermore, in SMKO mice the stretch at
224 both 5 mN and maximum force was significantly higher in the ascending aorta (S1) but
225 significantly lower in the descending aorta (S3) at maximum force (Figure 4B; Tables S9 and
226 S10).
227
228 ***Ltbp1*, *Mfap4*, and *Timp1* CRISPR/Cas9 Knock-In Mouse Models**
229 During the one-year period of aging, no *Ltbp1*, *Mfap4*, or *Timp1* CRISPR/Cas9 knock-in mice
230 died due to aortic rupture. Moreover, the rupture force of the aortic segments S1, S2, and S3
231 showed no considerable difference between wild-type controls and hetero-, homo-, or
232 hemizygous mice of *Ltbp1*, *Mfap4*, and *Timp1* CRISPR/Cas9 knock-in mice (Figure 5; Table
233 S11).
234
235

236 **DISCUSSION**

237 Inbred mouse hAD models are valuable tools for the investigation of medical therapeutic
238 approaches and the establishment of gene-disease association and have been widely adopted
239 for the identification of cardiovascular abnormalities by assessing aortic diameter,
240 morphology, and wall thickness as well as by considering histological staining, omics data, or
241 survival rate.[30-36] Although these methods provide observational insights, they cannot
242 directly/objectively reveal how medical therapy or sequence variants influence the strength
243 (i.e., rupture force) of the aortic wall at individual level. In this study, rupture force
244 measurements provide insights into the biomechanical integrity of the thoracic aorta in three
245 established (*Fbn1*^{C1041G}, *Fbn1*^{mgR}, and *Efemp2* SMKO) and three novel candidate-gene
246 (*Ltbp1*, *Mfap4*, and *Timp1*) mouse hAD models.

247 By applying the aortic rupture force measurement to both mouse MFS models (i.e., the
248 phenotypically milder heterozygous *Fbn1*^{C1041G} and the phenotypically more severe
249 homozygous *Fbn1*^{mgR} mice), we showed a significantly reduced rupture force compared to
250 wild-type littermates for the first time. The reduced rupture force is one indicator of impaired
251 biomechanical integrity, which was most noticeably present in the ascending aorta (S1 in
252 Figures 1A and 3A). The aortic wall of *Fbn1*$^{+/C1041G}$ mice is known to be normal in
253 (histological) appearance around 3 months of age, only showing evidence of medial
254 thickening and/or progressive deterioration within the medial layer, including elastic fiber
255 fragmentation in association with excess expression of matrix metalloproteinase 2 (MMP2)
256 and 9 (MMP9), at later ages.[17,18] However, our read-out system allowed the identification of
257 an impaired aortic wall integrity before 3 months of age (cf. *Fbn1*$^{+/C1041G}$ mice used in this
258 study were 10-week-old).

259 Compared to wild-type controls and in contrast to *Fbn1*$^{+/C1041G}$ mice, the ascending
260 aorta of *Fbn1*$^{mgR/mgR}$ mice showed significantly increased stretch at both 5 mN and maximum
261 force (cf. Figure 1B and Figure 3B; note that the stretch of ring-shaped S1-S3 reflects half the

262 circumference of the aorta and thus the aortic diameter). Increased aortic stretch was even
263 more pronounced in male than in female mice, which is in line with previously published
264 aortic diameters using ultrasound measurements.[37-38] Indeed, sex is a well-known risk factor
265 for cardiovascular diseases and several clinical studies have shown that sex also strongly
266 influences the outcome of MFS, with men having a higher risk for aortic dilatations and
267 arterial events.[39-41]

268 The antihypertensive drug losartan recognizably reduced S1 stretch, which reflects
269 aortic diameter, likely due to lowering blood pressure (spikes), but had no impact on S1-S3
270 rupture force in *Fbn1*$^{mgR/mgR}$ mice (Figure 3). This result implies that the thoracic aorta treated
271 with losartan remains susceptible to rupture despite the reduction in aortic stretch/diameter.
272 Consequently, aortic rupture force beyond aortic diameter may be useful for the investigation
273 of potential drug therapies in mouse models of hAD characterized by aneurysms. We propose
274 that our read-out system provides clinically-relevant information allowing novel insights into
275 the evaluation of medical therapies for the prevention of arterial events in hADs that cannot
276 be obtained by assessment of the aneurysm alone.

277 In the *Efemp2* SMKO mouse model, our data shows that the absence of Fbln4 in the
278 aortic ECM results in significantly reduced rupture force and increased stretch of the
279 ascending aorta, indicating impaired biomechanical integrity of the aortic wall (Figure 4).
280 This is likely related to the effect of Fbln4 on elastogenesis[42] and collagen biosynthesis[26]
281 involved in the development of ascending aortic aneurysms,[43,44] as previously described.
282 Considering that the ascending aorta is subjected to the highest hemodynamic stress, it is not
283 surprising that knock-out of *Efemp2* in vascular smooth muscle cells has a stronger effect on
284 the ascending than on the descending aorta (i.e., S1 compared to S2 and S3), despite the
285 higher elastin content of the ascending aorta.[45,46]

286 Compared to the previously reported *Col3a1*^{m1Lsmi} mouse vEDS model,[12,16] the aortic
287 rupture forces of both *Fbn1*$^{+/C1041G}$ and *Fbn1*$^{mgR/mgR}$ mouse MFS models were significantly

288 higher in all three aortic segments (Figure 6; Table S12). This relative aortic weakness of the
289 *Col3a1*$^{+/m1Lsmi}$ mice is consistent with their higher mortality rate compared with *Fbn1*$^{mgR/mgR}$
290 mice (Figure S3; note that survival rate does not reflect aortic rupture force at the individual
291 level, as not all mice with significantly reduced rupture force have a reduced survival). In
292 contrast, SMKO mice showed in the ascending aorta (S1) relative aortic rupture force values
293 comparable to or lower than those of mice modeling vEDS, but in the descending aorta (S2
294 and S3) the relative rupture force of SMKO mice was comparable to that of mice modeling
295 MFS (Figure 6; Table S12).

296 Given that our measurements demonstrated reduced aortic rupture force of established
297 hAD mouse models in this study (*Fbn1*^{C1041G}, *Fbn1*^{mgR}, and *Efemp2* SMKO) and elsewhere
298 (*Col3a1*^{m1Lsmi}),[12,16] we evaluated aortic rupture force in three CRISPR/Cas9-engineered mouse
299 models of hAD candidate genes as well. In humans, these three genes (*LTBP1*, *MFAP4*, and
300 *TIMP1*) are expressed at higher levels in arterial tissue than in any other tissue studied in
301 GTEx (gtexportal.org/home). LTBP1 interacts with ECM proteins, such as MFS-associated
302 FBN1, and regulates transforming growth factor (TGF)-β,[47] which plays an important role in
303 the pathogenesis of hADs.[48] MFAP4, an ECM protein found in elastic fibers, interacts with
304 FBN1, FBN2, and type I collagen as well as actively promotes tropoelastin self-assembly by
305 binding tropoelastin.[49] TIMP1 is a strong inhibitor of many MMPs, thereby preventing
306 excessive ECM degradation.[50] Knock-out mouse models of *Ltbp1*, *Mfap4*, and *Timp1* showed
307 cardiovascular phenotypes,[51-56] indicating that mutations in these genes could be causative for
308 hAD.

309 In contrast to established hAD mouse models (i.e., mice with mutation in the genes
310 *Fbn1*, *Efemp2*, or *Col3a1*), however, our read-out system revealed no significantly reduced
311 aortic rupture force for any genotypes of the three novel knock-in mouse models *Ltbp1*^{G1132S},
312 *Mfap4*^{D42A}, and *Timp1*^{I120T} at the age of 1 year (Figure 5). This indicates and clarifies the lack
313 of aortic significance of the human-equivalent sequence variants with unknown pathogenicity

knocked into our mouse models. The non-reduced aortic rupture forces of the three knock-in mouse models are consistent with their non-increased aortic stretch and non-reduced survival rate (data not shown). Further studies are needed to assess the clinical significance of the genes *LTBP1*, *MFAP4*, and *TIMP1* in hAD, also considering a disease-modifying (synergistic) effect of these genes as well as mice with a different genetic background.[57]

Taken together, this study demonstrates that the measurement of aortic rupture force can not only explain the aortic phenotype of established mouse hAD models but also clarify the unknown/uncertain aortic significance of candidate genes, variants, and drugs, thereby paving the way for better molecular diagnosis and medical therapies in hAD. Thus, rupture force can be a valuable parameter to consider in future studies of aortic aneurysms and dissections, especially in evaluating the beneficial effects of pharmacological therapies to attenuate the risk of these life-threatening conditions.

Acknowledgements

We thank Cyagen (Santa Clara, CA, USA) for help with the generation of the three CRISPR/Cas9 knock-in mouse models, Bryana M. Levitan for performing ultrasound measurements of *Fbn1*^{mgR} mice as well as Daniela Brkan, Edina Jusufi, Marc T. Schönholzer, Giancarlo Tomio, and Dzenneta Zukovic for help with data analysis and/or figure preparation.

Sources of Funding

This work was supported by the Isaac Dreyfus-Bernheim Stiftung and the Fondation pour la Recherche et le Traitement Médical (FRTM) as well as by NIH NHLBI (grant number K01 HL149984) and JSPS KAKENHI (grant number JP20H03762).

Disclosures

None.

Supplemental Material

Statistical Analyses

Figures S1-S3

Tables S1-S12

Major Resources Table

348 **REFERENCES**

349 1. Lindsay ME, Dietz HC. Lessons on the pathogenesis of aneurysm from heritable
350 conditions. *Nature*. 2011;473:308-316. doi: 10.1038/nature10145
351 2. Verstraeten A, Luyckx I, Loeys B. Aetiology and management of hereditary aortopathy.
352 *Nat Rev Cardiol*. 2017;14:197-208. doi: 10.1038/nrcardio.2016.211
353 3. Creamer TJ, Bramel EE, MacFarlane EG. Insights on the pathogenesis of aneurysm
354 through the study of hereditary aortopathies. *Genes*. 2021;12:183. doi:
355 10.3390/genes12020183
356 4. Caspar SM, Dubacher N, Kopps AM, Meienberg J, Henggeler C, Matyas G. Clinical
357 sequencing: From raw data to diagnosis with lifetime value. *Clin Genet*. 2018;93:508-
358 519. doi: 10.1111/cge.13190
359 5. Renard M, Francis C, Ghosh R, Scott AF, Witmer PD, Adès LC, Andelfinger GU,
360 Arnaud P, Boileau C, Callewaert BL, Guo D, Hanna N, Lindsay ME, Morisaki H,
361 Morisaki T, Pachter N, Robert L, Van Laer L, Dietz HC, Loeys BL, Milewicz DM, De
362 Backer J. Clinical Validity of Genes for Heritable Thoracic Aortic Aneurysm and
363 Dissection. *J Am Coll Cardiol*. 2018;72:605-615. doi: 10.1016/j.jacc.2018.04.089
364 6. Caspar SM, Dubacher N, Matyas G. More Genes for Thoracic Aortic Aneurysms and
365 Dissections. *J Am Coll Cardiol*. 2019;73:528-529. doi: 10.1016/j.jacc.2018.09.094
366 7. Humphrey JD, Milewicz DM, Tellides G, Schwartz MA. Dysfunctional mechanosensing
367 in aneurysms. *Science*. 2014;344:477-479. doi: 10.1126/science.1253026
368 8. Humphrey JD, Schwartz MA, Tellides G, Milewicz DM. Role of mechanotransduction in
369 vascular biology: focus on thoracic aortic aneurysms and dissections. *Circ Res*.
370 2015;116:1448-1461. doi: 10.1161/CIRCRESAHA.114.304936
371 9. Pierce DM, Maier F, Weisbecker H, Viertler C, Verbrugghe P, Famaey N, Fourneau I,
372 Herijgers P, Holzapfel GA. Human thoracic and abdominal aortic aneurysmal tissues:

Damage experiments, statistical analysis and constitutive modeling. *J Mech Behav Biomed Mater*. 2015;41:92-107. doi: 10.1016/j.jmbbm.2014.10.003

10. Chiu P, Lee H-P, Dalal AR, Koyano T, Nguyen M, Connolly AJ, Chaudhuri O, Fischbein MP. Relative strain is a novel predictor of aneurysmal degeneration of the thoracic aorta: An ex vivo mechanical study. *JVS Vasc Sci*. 2021;2:235-246. doi: 10.1016/j.jvssci.2021.08.003
11. Chittajallu SNSH, Richhariya A, Tse KM, Chinthapenta V. A Review on Damage and Rupture Modelling for Soft Tissues. *Bioengineering (Basel)*. 2022;9:26. doi: 10.3390/bioengineering9010026
12. Dubacher N, Münger J, Gorosabel MC, Crabb J, Ksiazek AA, Caspar SM, Bakker ENTP, van Bavel E, Ziegler U, Carrel T, Steinmann B, Zeisberger S, Meienberg J, Matyas G. Celiprolol but not losartan improves the biomechanical integrity of the aorta in a mouse model of vascular Ehlers-Danlos syndrome. *Cardiovasc Res*. 2019;16:457-465. doi: 10.21037/acs.2017.11.10
13. Ong K-T, Perdu J, De Backer J, Bozec E, Collignon P, Emmerich J, Fauret A-L, Fiessinger J-N, Germain DP, Georgesco G, Hulot J-S, De Paepe A, Plauchu H, Jeunemaitre X, Laurent S, Boutouyrie P. Effect of celiprolol on prevention of cardiovascular events in vascular Ehlers-Danlos syndrome: a prospective randomised, open, blinded-endpoints trial. *Lancet* 2010;376:1476-1484. doi: 10.1016/S0140-6736(10)60960-9
14. Frank M, Adham S, Seigle S, Legrand A, Mirault T, Henneton P, Albuisson J, Denarié N, Mazzella J-M, Mousseaux E, Messas E, Boutouyrie P, Jeunemaitre X. Vascular Ehlers-Danlos Syndrome: Long-Term Observational study. *J Am Coll Cardiol.* 2019;73:1948-1957. doi: 10.1016/j.jacc.2019.01.058

397 15. Baderkhan H, Wanhainen A, Stenborg A, Stattin E-L, Björck M. Celiprolol Treatment in
398 Patients with Vascular Ehlers-Danlos Syndrome. *Eur J Vasc Endovasc Surg.*
399 2021;61:326-331. doi: 10.1016/j.ejvs.2020.10.020
400 16. Gorosabel MC, Dubacher N, Meienberg J, Matyas G. Vascular Ehlers-Danlos syndrome:
401 can the beneficial effect of celiprolol be extrapolated to bisoprolol? *EHJ - Cardiovasc*
402 *Pharmacother*. 2020;6:199-200. doi: 10.1093/ehjcvp/pvz067
403 17. Judge DP, Biery NJ, Keene DR, Geubtner J, Myers L, Huso DL, Sakai LY, Dietz HC.
404 Evidence for a critical contribution of haploinsufficiency in the complex pathogenesis of
405 Marfan syndrome. *J Clin Invest*. 2004;114:172-181. doi: 10.1172/JCI20641
406 18. Pereira L, Lee SY, Gayraud B, Andrikopoulos K, Shapiro SD, Bunton T, Biery NJ, Dietz
407 HC, Sakai LY, Ramirez F. Pathogenetic sequence for aneurysm revealed in mice
408 underexpressing fibrillin-1. *Procl Natl Acad Sci U S A*. 1999;96:3819-3823. doi:
409 10.1073/pnas.96.7.3819
410 19. Bunton TE, Biery NJ, Myers L, Gayraud B, Ramirez F, Dietz HC. Phenotypic Alteration
411 of Vascular Smooth Muscle Cells Precedes Elastolysis in a Mouse Model of Marfan
412 Syndrome. *Circ Res*. 2001;88:37-43. doi: 10.1161/01.res.88.1.37
413 20. Saeyeldin A, Zafar MA, Velasquez CA, Ip K, Gryaznov A, Brownstein AJ, Li Y, Rizzo
414 JA, Erben Y, Ziganshin BA, Elefteriades JA. Natural history of aortic root aneurysms in
415 Marfan syndrome. *Ann Cardiothorac Surg*. 2017;6:625-632. doi:
416 10.21037/acs.2017.11.10
417 21. Habashi JP, Judge DP, Holm TM, Cohn RD, Loeys BL, Cooper TK, Myers L, Klein EC,
418 Liu G, Calvi C, Podowski M, Neptune ER, Halushka MK, Bedja D, Gabrielson K, Rifkin
419 DB, Carta L, Ramirez F, Huso DL, Dietz HC. Losartan, an AT1 Antagonist, Prevents
420 Aortic Aneurysm in a Mouse Model of Marfan Syndrome. *Science*. 2006;312:117-121.
421 doi: 10.1681/ASN.2006050508

422 22. Habashi JP, Doyle JJ, Holm TM, Aziz H, Schoenhoff F, Bedja D, Chen Y, Modiri AN,
423 Judge DP, Dietz HC. Angiotensin II Type 2 Receptor Signaling Attenuates Aortic
424 Aneurysm in Mice Through ERK Antagonism. *Science*. 2011;332:361-365. doi:
425 10.1126/science.1192152
426 23. Bhatt AB, Buck JS, Zuflacht JP, Milian J, Kadivar S, Gauvreau K, Singh MN, Creager
427 MA. Distinct effects of losartan and atenolol on vascular stiffness in Marfan syndrome.
428 *Vasc Med*. 2015;20:317-325. doi: 10.1177/1358863X15569868
429 24. Cook JR, Clayton NP, Carta L, Galatioto J, Chiu E, Smaldone S, Nelson CA, Cheng SH,
430 Wentworth BM, Ramirez F. Dimorphic effects of transforming growth factor-β signaling
431 during aortic aneurysm progression in mice suggest a combinatorial therapy for Marfan
432 syndrome. *Arterioscler Thromb Vasc Biol*. 2015;35:911-917. doi:
433 10.1161/ATVBAHA.114.305150
434 25. Robertson DM, Truong DT, Cox DA, Carmichael HL, Ou Z, Minich LL, Williams RV,
435 Selamet Tierney ES. Pediatric Heart Network Trial of Losartan vs. Atenolol in Children
436 and Young Adults with Marfan Syndrome: Impact on Prescription Practices. *Pediatr*
437 *Cardiol.* 2023;44:618-623. doi: 10.1007/s00246-022-02976-z
438 26. Huang J, Davis EC, Chapman SL, Budatha M, Marmorstein LY, Word RA, Yanagisawa
439 H. Fibulin-4 Deficiency Results in Ascending Aortic Aneurysms: A Potential Link
440 Between Abnormal Smooth Muscle Cell Phenotype and Aneurysm Progression. *Circ Res*.
441 2010;106:583-592. doi: 10.1161/CIRCRESAHA.109.207852
442 27. Hucthagowder V, Sausgruber N, Kim KH, Angle B, Marmorstein LY, Urban Z. Fibulin-
443 4: A Novel Gene for an Autosomal Recessive Cutis Laxa Syndrome. *Am J Hum Genet*.
444 2006;78:1075-1080. doi: 10.1086/504304
445 28. Renard M, Holm T, Veith R, Callewaert BL, Adès LC, Baspinar O, Pickart A, Dasouki
446 M, Hoyer J, Rauch A, Trapane P, Earing MG, Coucke PJ, Sakai LY, Dietz HC, De Paepe
447 AM, Loeys BL. Altered TGFβ signaling and cardiovascular manifestations in patients

448 with autosomal recessive cutis laxa type I caused by fibulin-4 deficiency. *Eur J Hum*
449 *Genet*. 2010;18:895-901. doi: 10.1038/ejhg.2010.45
450 29. Muthu ML, Tiedemann K, Fradette J, Komarova S, Reinhardt DP. Fibrillin-1 regulates
451 white adipose tissue development, homeostasis, and function. *Matrix Biol*.
452 2022;110:106-128. doi: 10.1016/j.matbio.2022.05.002
453 30. Lee VS, Halabi CM, Hoffman EP, Carmichael N, Leshchiner I, Lian CG, Bierhals AJ,
454 Vuzman D, Brigham Genomic Medicine, Mecham RP, Frank NY, Stitziel NO. Loss of
455 function mutation in *LOX* causes thoracic aortic aneurysm and dissection in humans. *Proc*
456 *Natl Acad Sci U S A*. 2016;113:8759-8764. doi: 10.1073/pnas.1601442113
457 31. Halabi CM, Broekelmann TJ, Lin M, Lee VS, Chu M-L, Mecham RP. Fibulin-4 is
458 essential for maintaining arterial wall integrity in conduit but not muscular arteries. *Sci*
459 *Adv*. 2017;3:e1602532. doi: 10.1126/sciadv.1602532
460 32. Parker SJ, Stotland A, MacFarlane E, Wilson N, Orosco A, Venkatraman V, Madrid K,
461 Gottlieb R, Dietz HC, Van Eyk JE. Proteomics reveals Rictor as a noncanonical TGF-β
462 signaling target during aneurysm progression in Marfan mice. *Am J Physiol Heart Circ*
463 *Physiol*. 2018;315:H1112-H1126. doi: 10.1152/ajpheart.00089.2018
464 33. Bhushan R, Altinbas L, Jäger M, Zaradzki M, Lehmann D, Timmermann B, Clayton NP,
465 Zhu Y, Kallenbach K, Kararigas G, Robinson PN. An integrative systems approach
466 identifies novel candidates in Marfan syndrome-related pathophysiology. *J Cell Mol Med*.
467 2019;23:2526-2535. doi: 10.1111/jcmm.14137
468 34. Bowen CJ, Calderón Giadrosic JF, Burger Z, Rykiel G, Davis EC, Helmers MR, Benke
469 K, Gallo MacFarlane E, Dietz HC. Targetable cellular signaling events mediate vascular
470 pathology in vascular Ehlers-Danlos syndrome. *J Clin Invest*. 2020;130:686-698. doi:
471 10.1172/JCI130730

472 35. Xiong W, Meisinger T, Knispel R, Worth JM, Baxter BT. MMP-2 Regulates Erk1/2
473 Phosphorylation and Aortic Dilatation in Marfan Syndrome. *Circ Res*. 2012;110:e92-
474 e101. doi: 10.1161/CIRCRESAHA.112.268268
475 36. Sheppard MB, Chen JZ, Rateri DL, Moorleghen JJ, Weiland M, Daugherty A. Renin-
476 Angiotensin System Inhibitors Do Not Improve Survival in Fibrillin-1 Hypomorphic
477 Mice with Established Aortic Aneurysm. *J Clin Trans Sci*. 2019;3:112-113. doi:
478 10.1017/cts.2019.258
479 37. Chen JZ, Rateri D, Sheppard M, Daugherty A. Abstract 20315: Sexual Dimorphism in a
480 Marfan Syndrome Mouse Model. *Circulation*. 2017;136:A20315.
481 38. Chen JZ, Sawada H, Moorleghen JJ, Weiland M, Daugherty A, Sheppard MB. Aortic
482 strain correlates with elastin fragmentation in fibrillin-1 hypomorphic mice. *Circ Rep*.
483 2019;1:199-205. doi: 10.1253/circrep.CR-18-0012
484 39. Détaint D, Faivre L, Collod-Beroud G, Child AH, Loeys BL, Binquet C, Gautier E,
485 Arbustini E, Mayer K, Arslan-Kirchner M, Stheneur C, Halliday D, Beroud C, Bonithon-
486 Kopp C, Claustres M, Plauchu H, Robinson PN, Kiotsekoglou A, De Backer J, Adès L,
487 Francke U, De Paepe A, Boileau C, Jondeau G. Cardiovascular manifestations in men and
488 women carrying a FBN1 mutation. *Eur Heart J*. 2010;31:2223-2229. doi:
489 10.1093/eurheartj/ehq258
490 40. Holmes KW, Maslen CL, Kindem M, Kroner BL, Song HK, Ravekes W, Dietz HC,
491 Weinsaft JW, Roman MJ, Devereux RB, Pyeritz RE, Bavaria J, Milewski K, Milewicz D,
492 LeMaire SA, Hendershot T, Eagle KA, Tolunay HE, Desvigne-Nickens P, Silberbach M,
493 for the GenTAC Registry Consortium. GenTAC registry report: Gender differences
494 among individuals with genetically triggered thoracic aortic aneurysm and dissection. *Am
495 J Med Genet*. 2013;161:779-786. doi: 10.1002/ajmg.a.35836

496 41. Renard M, Muiño-Mosquera L, Manalo EC, Tufa S, Carlson EJ, Keene DR, De Backer J,
497 Sakai LY. Sex, pregnancy and aortic disease in Marfan syndrome. *PLoS ONE*.
498 2017;12:e0181166. doi: 10.1371/journal.pone.0181166
499 42. Horiguchi M, Inoue T, Ohbayashi T, Hirai M, Noda K, Marmorstein LY, Yabe D, Takagi
500 K, Akama TO, Kita T, Kimura T, Nakamura T. Fibulin-4 conducts proper elastogenesis
501 via interaction with cross-linking enzyme lysyl oxidase. *Proc Natl Acad Sci U S A*.
502 2009;106:19029-19034. doi: 10.1073/pnas.0908268106
503 43. Papke CL, Yanagisawa H. Fibulin-4 and fibulin-5 in elastogenesis and beyond: Insights
504 from mouse and human studies. *Matrix Biol*. 2014;37:142-149. doi:
505 10.1016/j.matbio.2014.02.004
506 44. Papke CL, Tsunezumi J, Ringuette L-J, Nagaoka H, Terajima M, Yamashiro Y, Urquhart
507 G, Yamauchi M, Davis EC, Yanagisawa H. Loss of fibulin-4 disrupts collagen synthesis
508 and maturation: implications for pathology resulting from *EFEMP2* mutations. *Hum Mol*
509 *Genet*. 2015;24:5867-5879. doi: 10.1093/hmg/ddv308
510 45. Ruddy JM, Jones JA, Spinale FG, Ikonomidis JS. Regional heterogeneity within the
511 aorta: Relevance to aneurysm disease. *J Thorac Cardiovasc Surg*. 2008;136:1123-1130.
512 doi: 10.1016/j.jtcvs.2008.06.027
513 46. Jana S, Hu M, Shen M, Kassiri Z. Extracellular matrix, regional heterogeneity of the
514 aorta, and aortic aneurysm. *Exp Mol Med*. 2019;51:1-15. doi: 10.1038/s12276-019-0286-3
515 47. Morisaki T, Morisaki H. Genetics of hereditary large vessel diseases. *J Hum Genet*.
516 2016;61:21-26. doi: 10.1038/jhg.2015.119
517 48. Neptune ER, Frischmeyer PA, Arking DE, Myers L, Bunton TE, Gayraud B, Ramirez F,
518 Sakai LY, Dietz HC. Dysregulation of TGF-β activation contributes to pathogenesis in
519 Marfan syndrome. *Nat Genet*. 2003;33:407-411. doi: 10.1038/ng1116
520 49. Pilecki B, Holm AT, Schlosser A, Moeller JB, Wohl AP, Zuk AV, Heumüller SE, Wallis
521 R, Moestrup SK, Sengle G, Holmskov U, Sorensen GL. Characterization of

522 Microfibrillar-associated Protein 4 (MFAP4) as a Tropoelastin- and Fibrillin-binding
523 Protein Involved in Elastic Fiber Formation. *J Biol Chem*. 2016;291:1103-1114. doi:
524 10.1074/jbc.M115.681775
525 50. Brew K, Nagase H. The tissue inhibitors of metalloproteinases (TIMPs): An ancient
526 family with structural and functional diversity. *Biochim Biophys Acta*. 2010;1803:55-71.
527 doi: 10.1016/j.bbamcr.2010.01.003
528 51. Roten L, Nemoto S, Simsic J, Coker ML, Rao V, Baicu S, Defreyte G, Soloway PJ, Zile
529 MR, Spinale FG. Effects of Gene Deletion of the Tissue Inhibitor of the Matrix
530 Metalloproteinase-type 1 (TIMP-1) on Left Ventricular Geometry and Function in Mice.
531 *J Mol Cell Cardiol*. 2000;32:109-120. doi: 10.1006/jmcc.1999.1052
532 52. Eskandari MK, Vijungco JD, Flores A, Borensztajn J, Shively V, Pearce WH. Enhanced
533 abdominal aortic aneurysm in TIMP-1-deficient mice. *J Surg Res*. 2005;123:289-293. doi:
534 10.1016/j.jss.2004.07.247
535 53. Todorovic V, Frendewey D, Gutstein DE, Chen Y, Freyer L, Finnegan E, Liu F, Murphy
536 A, Valenzuela D, Yancopoulos G, Rifkin DB. Long form of latent TGF-β binding protein
537 1 (Ltbp1L) is essential for cardiac outflow tract septation and remodeling. *Development*.
538 2007;134:3723-3732. doi: 10.1242/dev.008599
539 54. Todorovic V, Finnegan E, Freyer L, Zilberberg L, Ota M, Rifkin DB. Long form of latent
540 TGF-β binding protein 1 (Ltbp1L) regulates cardiac valve development. *Dev Dyn*.
541 2011;240:176-187. doi: 10.1002/dvdy.22521
542 55. Schlosser A, Pilecki B, Hemstra LE, Kejling K, Kristmannsdottir GB, Wulf-Johansson H,
543 Moeller JB, Füchtbauer E-M, Nielsen O, Kirketerp-Møller K, Dubey LK, Hansen PBL,
544 Stubbe J, Wrede C, Hegermann J, Ochs M, Rathkolb B, Schrewe A, Bekeredjian R, Wolf
545 E, Gailus-Durner V, Fuchs H, Hrabě de Angelis M, Lindholt JS, Holmskov U, Sorensen
546 GL. MFAP4 Promotes Vascular Smooth Muscle Migration, Proliferation and Accelerates

547 Neointima Formation. *Arterioscler Thromb Vasc Biol*. 2016;36:122-133. doi:
548 10.1161/ATVBAHA.115.306672
549 56. Arpino V, Brock M, Gill SE. The role of TIMPs in regulation of extracellular matrix
550 proteolysis. *Matrix Biol*. 2015;44-46:247-254. doi: 10.1016/j.matbio.2015.03.005
551 57. Ritskes-Hoitinga M, Leenaars C, Beumer W, Coenen-de Roo T, Stafleu F, Meijboom
552 FLB. Improving Translation by Identifying Evidence for More Human-Relevant
553 Preclinical Strategies. *Animals*. 2020;10:1170. doi: 10.3390/ani10071170
554

555 **Highlights**

556 - Assay to measure the aortic rupture force as read-out for the biomechanical integrity
557 identified weakened murine thoracic aorta prior to micro- and macroscopic changes in
558 *Fbn1*$^{+/C1041G}$ mice.
559 - Despite reducing aneurysm growth, losartan treatment did not have any impact on the
560 aortic rupture force of *Fbn1*$^{mgR/mgR}$ mice modeling MFS.
561 - Smooth-muscle-cell-knock-out of *Efemp2* significantly impaired the rupture force of
562 the murine ascending aorta.
563 - Aortic rupture force measurements could clarify the causality of novel candidate
564 gene(s)/variant(s) in mouse models of aortic diseases.

Graphical Abstract

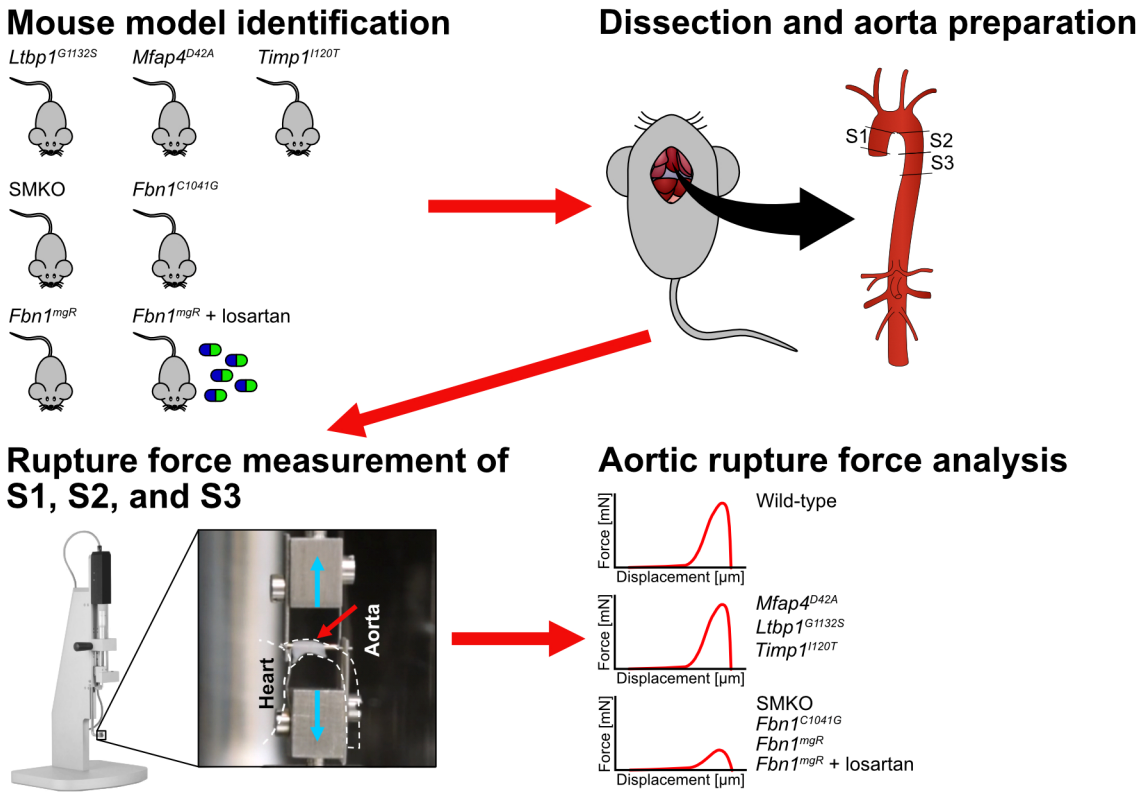

Figures and Figure Legends

Figure 1

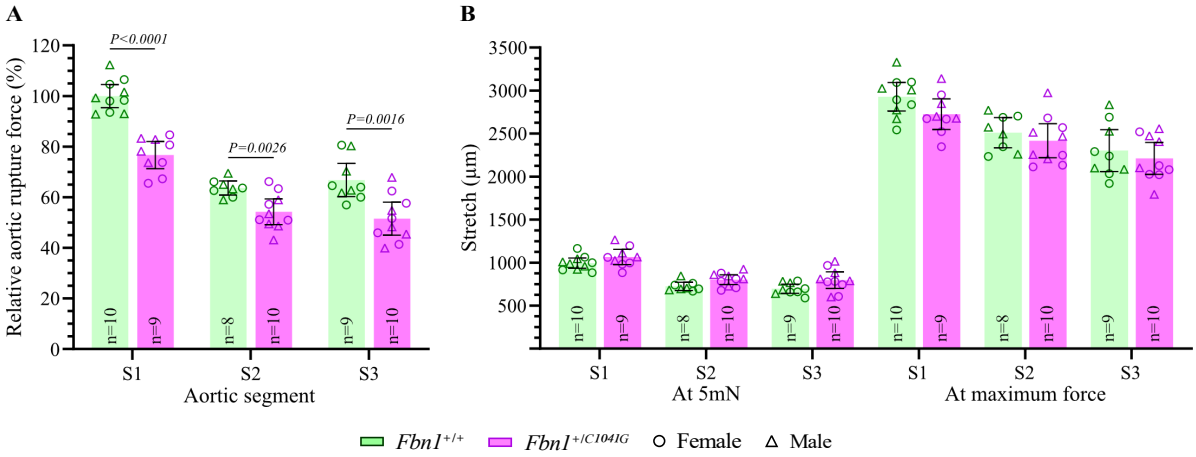

Figure 1. Aortic parameters of the *Fbn1*^{C1041G} mouse model.
A, Relative aortic rupture force (%) of three aortic segments (S1-S3) of 10-week-old *Fbn1*$^{+/+}$ and *Fbn1*$^{+/C1041G}$ mice. **B**, Stretch (in µm) of aortic segments at 5 mN (load-free aortic diameter) and maximum force of 10-week-old *Fbn1*$^{+/+}$ and *Fbn1*$^{+/C1041G}$ mice. Bars represent arithmetic means and error bars indicate 95% confidence intervals. The sample size (n) is displayed (damaged segments and outliers, i.e. >2× standard deviation, were excluded). For mean values with non- or slightly overlapping 95% CIs compared in text, two-tailed *P* values of unpaired t-tests are shown (applies to **A** only).

Figure 2

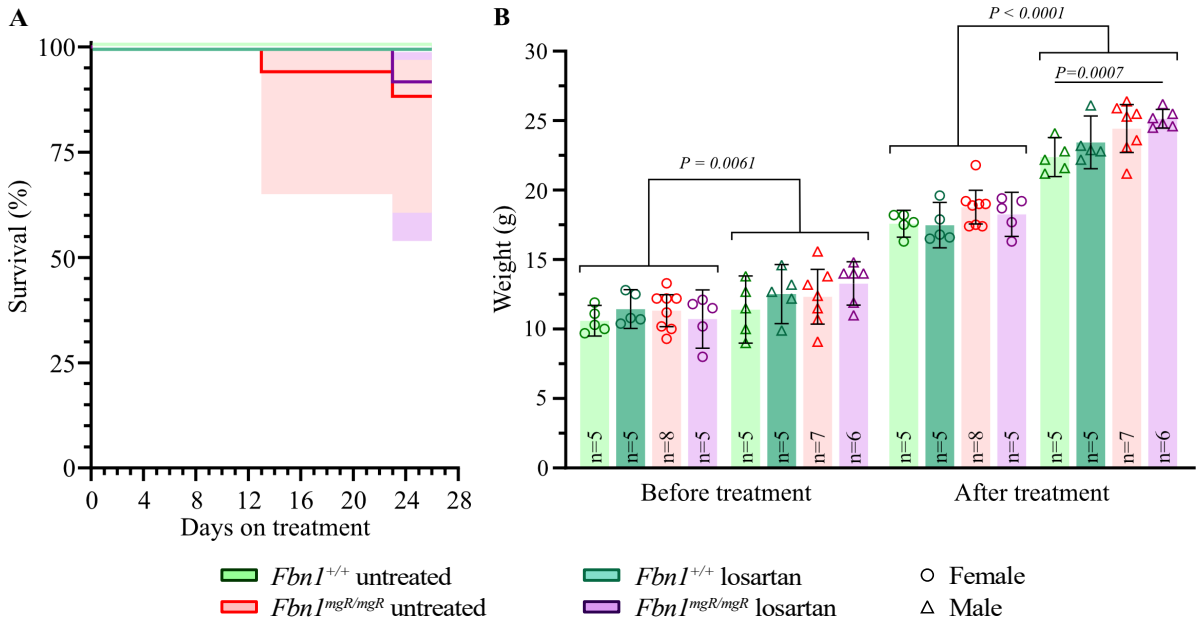

Figure 2. Survival and bodyweight of the *Fbn1*^{mgR} mouse model treated with the AGTR1-inhibitor losartan.
A, Kaplan-Meier curve for the survival of untreated *Fbn1*$^{+/+}$ mice (n=10) and *Fbn1*$^{mgR/mgR}$ mice (n=17), and *Fbn1*$^{+/+}$ (n=10) and *Fbn1*$^{mgR/mgR}$ (n=12) mice receiving losartan between the age of 4 and 8 weeks. Note that the survival curve of losartan-treated *Fbn1*$^{+/+}$ mice is masked by that of untreated *Fbn1*$^{+/+}$ mice. 95% confidence intervals (shaded areas) are shown for *Fbn1*$^{mgR/mgR}$ mice with survivals differing from 100%. **B**, Bodyweights of mice surviving the treatment period of 4 weeks measured before and after treatment at the age of 4 and 8 weeks, respectively. Bars represent arithmetic means, error bars indicate 95% confidence intervals. Significant two-tailed *P* values of unpaired t-tests are shown ($P<0.05$). For the comparison between female and male mice, the respective groups were pooled prior to *P* value calculation.

Figure 3

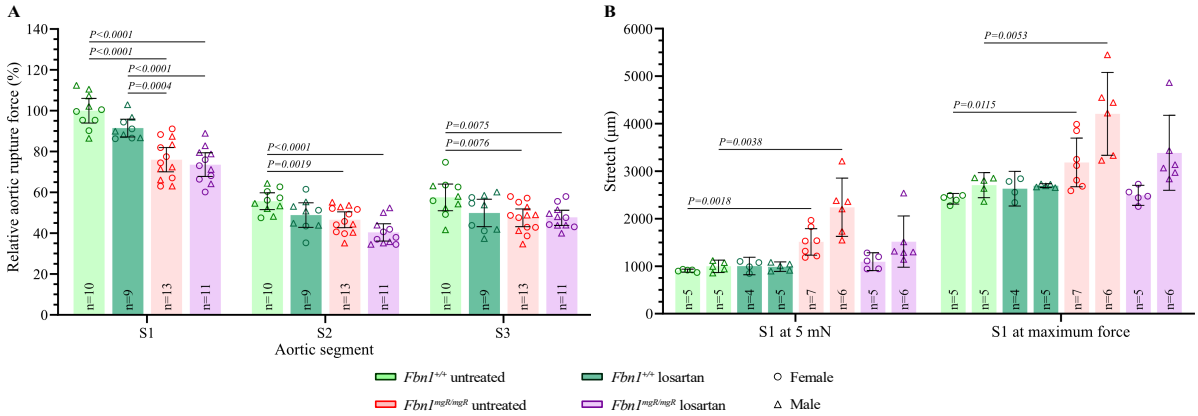

Figure 3. Aortic parameters of the *Fbn1*^{mgR} mouse model treated with the AGTR1-inhibitor losartan.
A, Relative aortic rupture force (%) of three aortic segments (S1-S3) of 8-week-old *Fbn1*$^{+/+}$ and *Fbn1*$^{mgR/mgR}$ mice after 4-week-long treatment with losartan. Untreated *Fbn1*$^{+/+}$ and *Fbn1*$^{mgR/mgR}$ mice served as control. **B**, Stretch (in µm) of the aortic segment S1 at 5 mN (load-free aortic diameter) as well as at maximum force in losartan-treated and untreated *Fbn1*$^{+/+}$ and *Fbn1*$^{mgR/mgR}$ mice separated according to sex. Bars represent arithmetic means and error bars indicate 95% confidence intervals (95% CI). The sample size (n) is displayed (damaged segments and outliers, i.e. >2× standard deviation, were excluded). For mean values with non- or slightly overlapping 95% CIs compared in text, two-tailed *P* values of unpaired t-tests are shown.

Figure 4

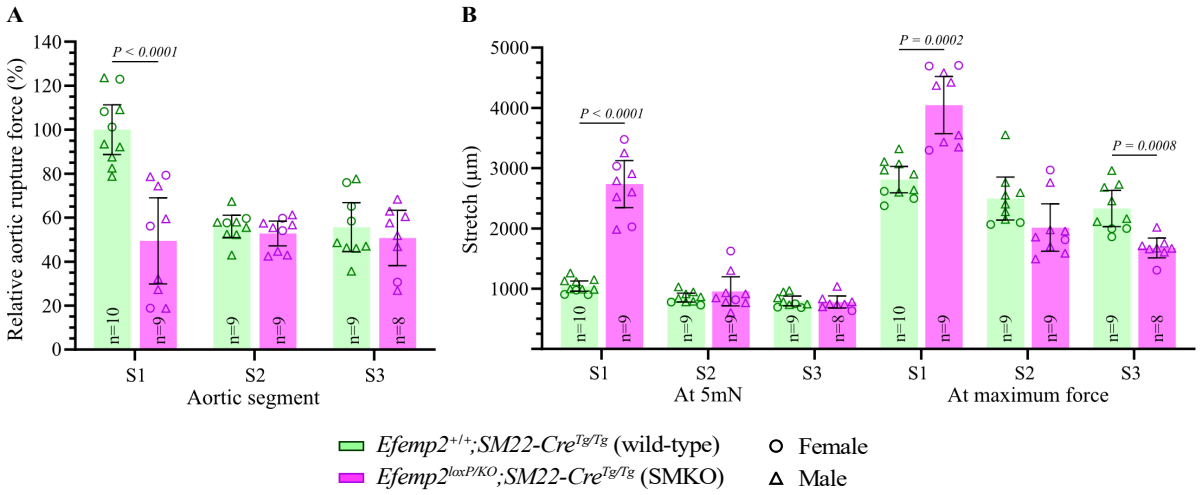

Figure 4. Aortic parameters of the *Efemp2* SMKO mouse model.
A, Relative aortic rupture force (%) of three aortic segments (S1-S3) of 8-week-old wild-type and SMKO mice. **B**, Stretch (in µm) of aortic segments at 5 mN (load-free aortic diameter) as well as at maximum force in wild-type and SMKO mice. Bars represent arithmetic means and error bars indicate 95% confidence intervals. The sample size (n) is displayed (damaged segments and outliers, i.e. >2× standard deviation, were excluded). For mean values with non- or slightly overlapping 95% CIs compared in text, two-tailed *P* values of unpaired t-tests are shown.

Figure 5

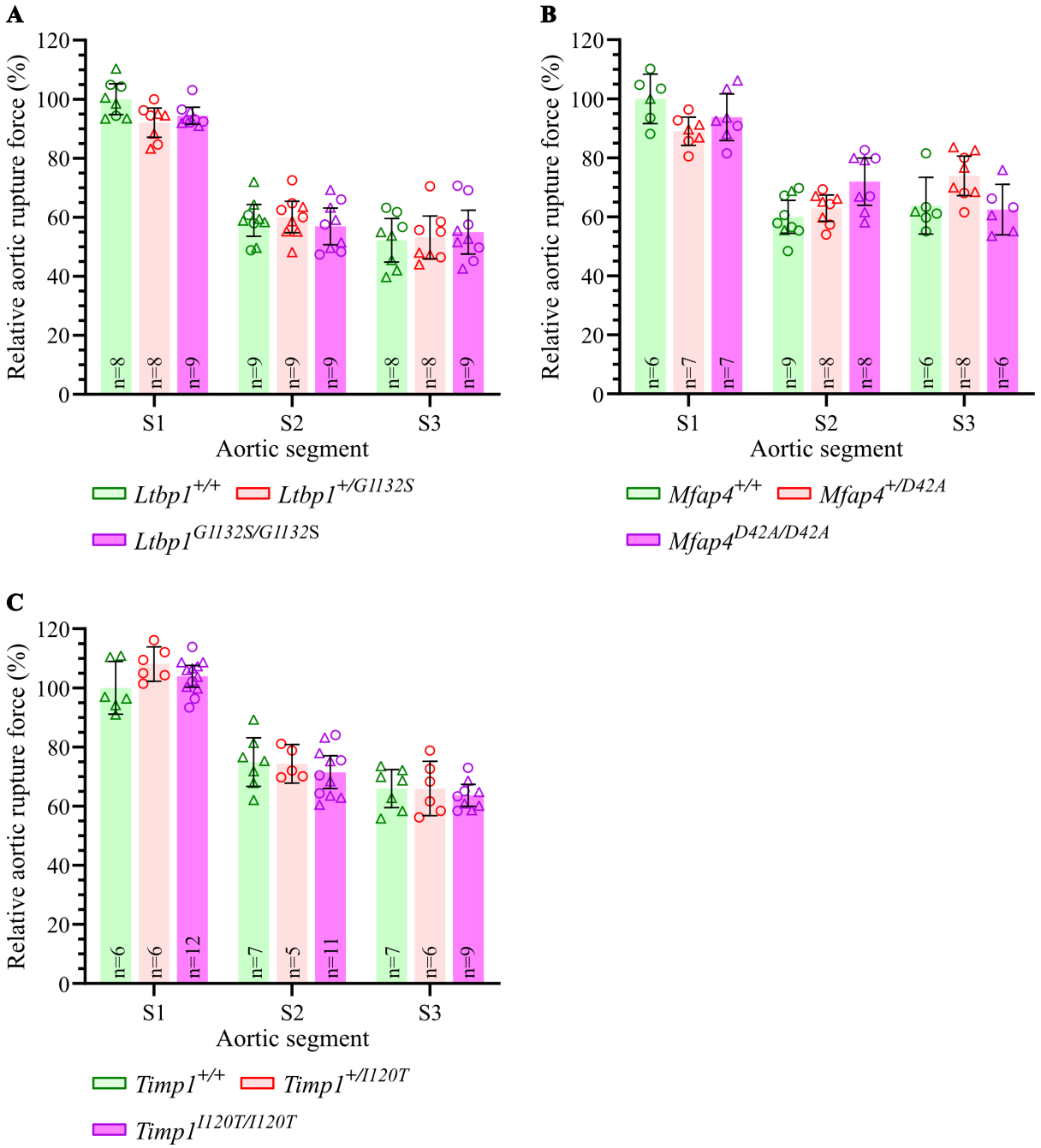

Figure 5. Aortic rupture force of the *Ltbp1*, *Mfap4*, and *Timp1* CRISPR/Cas9 knock-in mouse models.
A-C, Relative aortic rupture force (%) of three aortic segments (S1-S3) of 1-year-old wild-type and hetero- as well as hemi- and homozygous *Ltbp1* (**A**), *Mfap4* (**B**), and *Timp1* (**C**) CRISPR/Cas9 knock-in mice. Bars represent arithmetic means, error bars indicate 95% confidence intervals. The sample size (n) is displayed and damaged segments and outliers (>2× standard deviation) were excluded. Note the absence of non- or slightly overlapping 95% CIs per aortic segment. Circle, female; triangle, male.

Figure 6

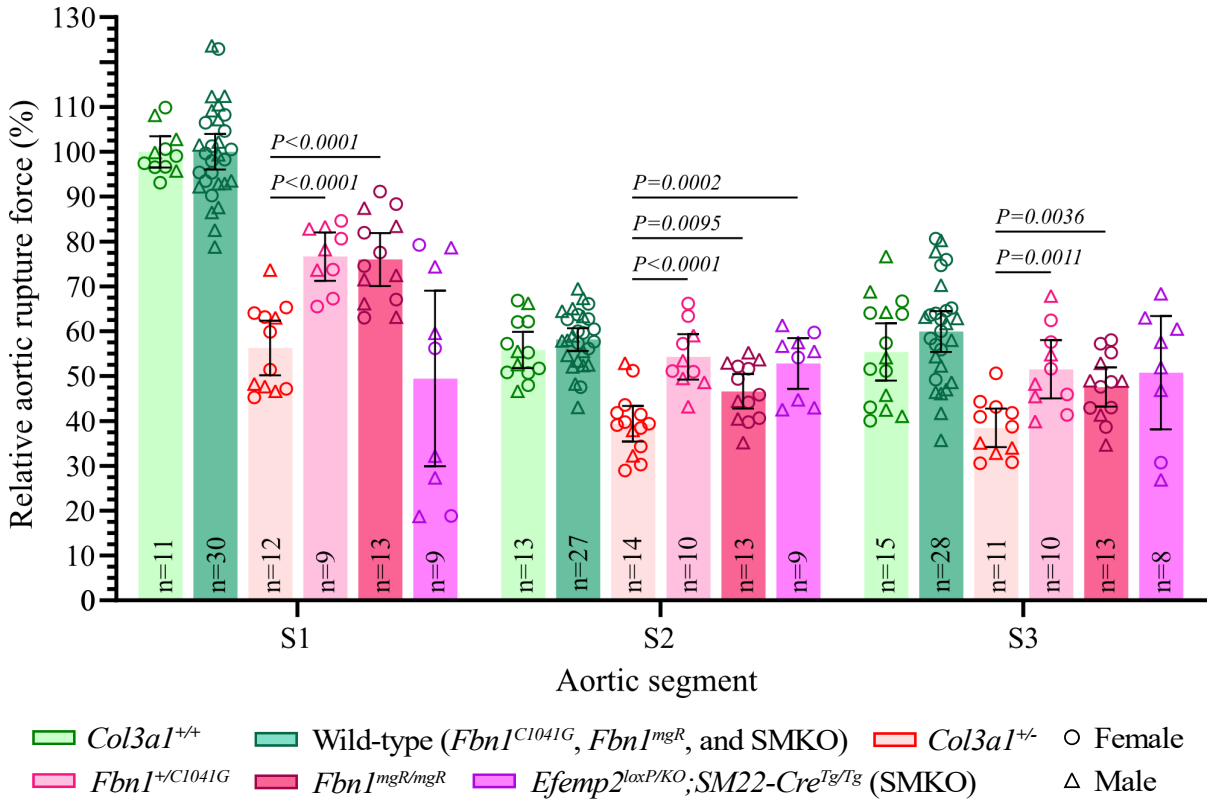

Figure 6. Aortic rupture force of the *Fbn1*^{C1041G}, *Fbn1*^{mgR}, and *Efemp2* SMKO mouse models compared to *Col3a1*^{m1Lsmi} mice modeling vEDS.

Relative aortic rupture force (%) of three aortic segments (S1-S3) of the mouse models *Col3a1*^{m1Lsmi} (data as described previously),[12] *Fbn1*^{C1041G}, *Fbn1*^{mgR}, and *Efemp2* SMKO (cf. wild-type controls of the *Fbn1*^{C1041G}, *Fbn1*^{mgR}, and *Efemp2* SMKO mouse models were pooled). Bars represent arithmetic means, error bars indicate 95% confidence intervals, The sample size (n) is displayed (damaged segments and outliers, i.e. >2× standard deviation, were excluded). For mean values with non- or slightly overlapping 95% CIs compared in text, two-tailed *P* values of unpaired t-tests are shown. *Col3a1*$^{+/+}$ and *Col3a1*$^{+/-}$ denotes wild-type and heterozygous mice of the *Col3a1*^{m1Lsmi} mouse model, respectively.